Coupled-mode-theory framework for nonlinear resonators comprising graphene

Thomas Christopoulos,[1,*] Odysseas Tsilipakos,[2,†] Nikolaos Grivas,[1] and Emmanouil E. Kriezis[1]
[1]*Department of Electrical and Computer Engineering, Aristotle University of Thessaloniki (AUTH), Thessaloniki 54124, Greece*
[2]*Institute of Electronic Structure and Laser, Foundation for Research and Technology Hellas (FORTH), Heraklion 71110, Crete, Greece*
(Received 16 September 2016; revised manuscript received 4 November 2016; published 27 December 2016)

A general framework combining perturbation theory and coupled-mode theory is developed for analyzing nonlinear resonant structures comprising dispersive bulk and sheet materials. To allow for conductive sheet materials, a nonlinear current term is introduced in the formulation in addition to the more common nonlinear polarization. The framework is applied to model bistability in a graphene-based traveling-wave resonator system exhibiting third-order nonlinearity. We show that the complex conductivity of graphene disturbs the equality of electric and magnetic energies on resonance (a condition typically taken for granted), due to the reactive power associated with the imaginary part of graphene's surface conductivity. Furthermore, we demonstrate that the dispersive nature of conductive materials must always be taken into account, since it significantly impacts the nonlinear response. This is explained in terms of the energy stored in the surface current, which is zeroed-out when linear dispersion is neglected. The results obtained with the proposed framework are compared with full-wave nonlinear finite-element simulations with excellent agreement. Very low characteristic power for bistability is obtained, indicating the potential of graphene for nonlinear applications.

DOI: 10.1103/PhysRevE.94.062219

I. INTRODUCTION

Nonlinear resonators are indispensable components for building functional photonic circuits. For example, resonant structures combining optical feedback with third-order nonlinearities give rise to a multitude of interesting phenomena, namely optical bistability (leading to memory [1], switching [2,3], and logic gate [4,5] functions), self-pulsation [6] (optical clock applications), and excitability [7] (neural network computing).

To date, mainly bulk materials (semiconductors, nonlinear polymers, chalcogenide glasses, etc.) are being incorporated in resonant structures to introduce nonlinearity. However, interest has recently shifted to sheet [two-dimensional (2D)] materials. In particular, graphene is already being employed in resonators [8–10] to provide nonlinearity and tunability. A robust framework for efficiently and accurately modeling nonlinear effects in resonators comprising graphene is thus in order. In this work, we address this need by developing a formulation combining perturbation theory and temporal coupled-mode theory (CMT). Unlike previous approaches [11–13], we allow for both bulk and sheet nonlinear materials by introducing a nonlinear current term in the formulation in addition to the more common nonlinear polarization. This way, graphene can be naturally modeled as an infinitesimally thin material, avoiding erroneous results and excessive computational burden [14]. Importantly, we also allow for material dispersion (in the linear properties) since graphene is highly dispersive, something that is shown to significantly affect the nonlinear response.

Besides being very efficient compared to nonlinear full-wave simulations, the proposed framework allows for obtaining robust design rules and gaining physical insight. We test its performance by considering optical bistability with a 2D resonator-waveguide system consisting of a graphene (or carbon) tube resonator coupled to a graphene sheet waveguide. Excellent agreement with full-wave simulations is obtained. In addition, high-quality bistable response with low input power is demonstrated, indicating the potential of graphene for nonlinear applications.

In our graphene-based example, the nonlinear current term is used to model the third-order nonlinearity originating from the nonlinear response of free electrons [15], which is analogous to the Kerr nonlinearity originating from the nonlinear motion of bound electrons in dielectric media [16]. In general, the presence of the nonlinear current term in the formulation can allow for studying any surface or bulk nonlinearity in conductive materials, whose nonlinear response is less examined compared to dielectric ones.

II. THEORETICAL FRAMEWORK

To derive a closed-form expression for the nonlinear frequency shift, we begin from Maxwell's equations in the frequency domain (spatial dependance is suppressed) for the unperturbed [Eqs. (1a) and (1b)] and perturbed [Eqs. (1c) and (1d)] case,

$$\nabla \times \mathbf{E_0} = -j\omega_0\mu_0\mathbf{H_0}, \tag{1a}$$

$$\nabla \times \mathbf{H_0} = j\omega_0\varepsilon_0\bar{\varepsilon}_r(\omega_0)\mathbf{E_0} + \bar{\sigma}^{(1)}(\omega_0)\mathbf{E_0}, \tag{1b}$$

$$\nabla \times \mathbf{E} = -j\omega\mu_0\mathbf{H}, \tag{1c}$$

$$\nabla \times \mathbf{H} = j\omega\varepsilon_0\bar{\varepsilon}_r(\omega)\mathbf{E} + \bar{\sigma}^{(1)}(\omega)\mathbf{E} + j\omega\mathbf{P_{NL}} + \mathbf{J_{NL}}, \tag{1d}$$

where we have adopted an $\exp\{+j\omega t\}$ harmonic convention and allowed for the general case of diagonally anisotropic materials. Following the conjugated form of the

*cthomasa@ece.auth.gr
†otsilipakos@iesl.forth.gr

reciprocity theorem [17,18], we calculate the divergence of $\mathbf{F_c} = \mathbf{E_0^*} \times \mathbf{H} + \mathbf{E} \times \mathbf{H_0^*}$:

$$\begin{aligned}\nabla \cdot \mathbf{F_c} = &-j(\omega-\omega_0)\mu_0 \mathbf{H}\cdot\mathbf{H_0^*} \\ &- j[\omega\overline{\varepsilon}_r(\omega) - \omega_0\overline{\varepsilon}_r^*(\omega_0)]\varepsilon_0 \mathbf{E}\cdot\mathbf{E_0^*} \\ &- [\overline{\sigma}^{(1)}(\omega) + \overline{\sigma}^{(1)*}(\omega_0)]\mathbf{E}\cdot\mathbf{E_0^*} \\ &- j\omega\mathbf{P_{NL}}\cdot\mathbf{E_0^*} - \mathbf{J_{NL}}\cdot\mathbf{E_0^*}. \end{aligned} \quad (2)$$

Since we are interested in specifying the nonlinear frequency shift (and not potential effects on the linewidth of the resonance [19]), we set $\overline{\varepsilon}_{r,\mathrm{Im}} = 0$ (henceforth, $\overline{\varepsilon}_r$ denotes the real part of the permittivity tensor) and $\overline{\sigma}^{(1)}_{\mathrm{Re}} = 0$ in Eq. (2), momentarily disregarding linear losses. Note that the effect of any nonlinear loss mechanism (e.g., two-photon absorption), rendering the frequency shift complex can be accounted for through complex nonlinear susceptibilities/conductivities. We next expand both relative permittivity and electrical conductivity tensors in Taylor series keeping only the first two terms, yielding $\omega\overline{\varepsilon}_r(\omega) = \omega_0\overline{\varepsilon}_r(\omega_0) + (\omega-\omega_0)\partial\{\omega\overline{\varepsilon}_r\}/\partial\omega|_{\omega=\omega_0}$ and $\overline{\sigma}^{(1)}_{\mathrm{Im}}(\omega) = \overline{\sigma}^{(1)}_{\mathrm{Im}}(\omega_0) + (\omega-\omega_0)\partial\{\overline{\sigma}^{(1)}_{\mathrm{Im}}\}/\partial\omega|_{\omega=\omega_0}$. Using, finally, Gauss's divergence theorem in an appropriately selected d-dimensional domain Ω ($d = \{2,3\}$), enclosed by the $(d-1)$-dimensional boundary Γ with a normal outward vector $\mathbf{n}$, such that $\int_\Omega \nabla\cdot\mathbf{F_c}\, d^d r = \oint_\Gamma \mathbf{F_c}\cdot\mathbf{n}\, d^{d-1}r = 0$ [20], Eq. (2) becomes

$$\begin{aligned} 0 = &-j\Delta\omega\int \mu_0\mathbf{H}\cdot\mathbf{H_0^*}d^dr - j\Delta\omega\int \varepsilon_0\frac{\partial\{\omega\overline{\varepsilon}_r\}}{\partial\omega}\mathbf{E}\cdot\mathbf{E_0^*}d^dr \\ &- j\Delta\omega\int \frac{\partial\overline{\sigma}^{(1)}_{\mathrm{im}}}{\partial\omega}\mathbf{E}\cdot\mathbf{E_0^*}d^dr \\ &- j\omega\int \mathbf{P_{NL}}\cdot\mathbf{E_0^*}d^dr - \int \mathbf{J_{NL}}\cdot\mathbf{E_0^*}d^dr, \end{aligned} \quad (3)$$

where $\Delta\omega = \omega - \omega_0$ is the resonance frequency shift due to all possible nonlinearities. All derivatives involved are calculated at $\omega = \omega_0$ with the notation suppressed for brevity. Equation (3) can be solved for $\Delta\omega$ yielding

$$\frac{\Delta\omega}{\omega_0} = -\frac{\int \mathbf{P_{NL}}\cdot\mathbf{E_0^*}d^dr - j\frac{1}{\omega_0}\int \mathbf{J_{NL}}\cdot\mathbf{E_0^*}d^dr}{\int \frac{\partial\left\{\varepsilon_0\omega\overline{\varepsilon}_r + \overline{\sigma}^{(1)}_{\mathrm{Im}}\right\}}{\partial\omega}\mathbf{E_0}\cdot\mathbf{E_0^*}d^dr + \mu_0\int \mathbf{H_0}\cdot\mathbf{H_0^*}d^dr}, \quad (4)$$

where we have assumed that $\mathbf{E} \approx \mathbf{E_0}$, $\mathbf{H} \approx \mathbf{H_0}$, and $\omega \approx \omega_0$, as first-order perturbation theory implies [12]. Equation (4) is general, describing the nonlinear frequency shift arising from polarization and/or current density nonlinearities. It additionally incorporates the dispersion of linear properties (electrical permittivity and conductivity).

Note that Eq. (4) reduces to the expressions derived in Refs. [11,21] when resonators comprising nondispersive bulk materials with isotropic $\chi^{(3)}$ susceptibilities are considered. Then

$$\Delta\omega_b = -\frac{1}{4}\left(\frac{\omega_0}{c_0}\right)^d c_0\omega_0\kappa_b n_2^{\max} W, \quad (5)$$

where $W = (\varepsilon_0/2)\int \varepsilon_r|\mathbf{E}_0|^2 d^dr$ is the total stored energy in the cavity, $n_2^{\max}$ is the maximum value of n_2 in the entire structure, and κ_b is a dimensionless nonlinear feedback parameter measuring the overlap between the resonant mode and the bulk nonlinear material [11] defined through

$$\kappa_b = \left(\frac{c_0}{\omega_0}\right)^d \frac{\frac{1}{3}\int \varepsilon_r n_2[2|\mathbf{E_0}|^4 + |\mathbf{E_0}\cdot\mathbf{E_0}|^2]d^dr}{\left[\frac{1}{2}\int \varepsilon_r|\mathbf{E_0}|^2 d^dr\right]^2 n_2^{\max}}. \quad (6)$$

Importantly, it was possible to eliminate the magnetic field in the denominator of Eq. (4) by using $W = W_e + W_m = 2W_e$, stating that electric and magnetic energies are equal on resonance. This does not always hold, as will be shown in what follows.

It is the second term in the numerator of Eq. (4) that can be used to incorporate nonlinear conductive sheet materials expanding the existing framework. Specifically, graphene exhibits a surface electrical conductivity consisting of a linear $\overline{\sigma}_s^{(1)}$ and a third-order nonlinear $\overline{\sigma}_s^{(3)}$ contribution, measured in S and S$(\mathrm{m/V})^2$, respectively. Linear conductivity induces a surface current density $\mathbf{J}_s = \sigma_1\mathbf{E}_{\mathbf{0},\parallel}$, where σ_1 is the only independent component of the $\overline{\sigma}_s^{(1)}$ tensor, and $\mathbf{E}_{\mathbf{0},\parallel}$ are the tangential to the graphene sheet components of $\mathbf{E_0}$. The nonlinear conductivity tensor $\overline{\sigma}_s^{(3)}$ has, in its simplest form, eight nonzero elements, all interacting exclusively with the tangential to the graphene sheet components of the electric field; only one of them is independent and is denoted with σ_3. Thus, the nonlinear current density in graphene is [14]

$$\mathbf{J_{NL}} = \frac{\sigma_3}{4}[2(\mathbf{E}_{\mathbf{0},\parallel}\cdot\mathbf{E}^*_{\mathbf{0},\parallel})\mathbf{E}_{\mathbf{0},\parallel} + (\mathbf{E}_{\mathbf{0},\parallel}\cdot\mathbf{E}_{\mathbf{0},\parallel})\mathbf{E}^*_{\mathbf{0},\parallel}]\delta_s(\mathbf{r}), \quad (7)$$

where $\delta_s(\mathbf{r})$ is a $(d-1)$-dimensional surface Dirac function.

For the THz regime we will be considering, the linear conductivity of graphene is dominated by the intraband term, exhibiting a strong Drude dispersion [14,22,23],

$$\sigma_1 = -j\frac{e^2\mu_c}{\pi\hbar^2(\omega - j/\tau_1)}\frac{2k_BT}{\mu_c}\ln\left[2\cosh\left(\frac{\mu_c}{2k_BT}\right)\right], \quad (8)$$

where e is the electron charge, $\hbar$ is the reduced Planck's constant, k_B is Boltzmann's constant, $T = 300$ K is the absolute temperature, $\tau_1 = 40$ ps is the relaxation time for intraband absorption in the THz regime, and μ_c is the chemical potential. $\sigma_1 = \sigma_{1,\mathrm{Re}} + j\sigma_{1,\mathrm{Im}}$ is complex, with $\sigma_{1,\mathrm{Im}} < 0$. The nonlinear conductivity is purely imaginary, meaning that no nonlinear loss mechanism (e.g., two-photon absorption) is present, and is given by [14,15]

$$\sigma_3 = j\frac{3e^4\upsilon_F^2}{32\omega^3\hbar^2\mu_c}, \quad (9)$$

where $\upsilon_F \approx c_0/300$ is the Fermi velocity in graphene. Note that $\sigma_{3,\mathrm{Im}}$ is always positive when $\mu_c > 0$.

Plugging Eq. (7) into Eq. (4) and neglecting both the polarization term and the permittivity dispersion, we reach

$$\Delta\omega_s = j\frac{\frac{1}{4}\int \sigma_3(2|\mathbf{E_{0,\parallel}}|^4+|\mathbf{E_{0,\parallel}}\cdot\mathbf{E_{0,\parallel}}|^2)d^{d-1}r}{\int(\varepsilon_0\varepsilon_r|\mathbf{E_0}|^2+\mu_0|\mathbf{H_0}|^2)d^dr+\int\frac{\partial\sigma_{1,\mathrm{Im}}}{\partial\omega}|\mathbf{E_{0,\parallel}}|^2d^{d-1}r}. \tag{10}$$

The integral in the numerator and the second integral in the denominator of Eq. (10) are reduced by one order since graphene is a sheet material as denoted by the $\delta_s(\mathbf{r})$ function. In direct analogy with the bulk case, a surface nonlinear feedback parameter κ_s can be defined as

$$\kappa_s = \left(\frac{c_0}{\omega_0}\right)^{d+1}\frac{\int\sigma_3(2|\mathbf{E_{0,\parallel}}|^4+|\mathbf{E_{0,\parallel}}\cdot\mathbf{E_{0,\parallel}}|^2)d^{d-1}r}{\left[\int(\varepsilon_r|\mathbf{E_0}|^2+\eta_0^2|\mathbf{H_0}|^2)d^dr+\frac{1}{\varepsilon_0}\int\frac{\partial\sigma_{1,\mathrm{Im}}}{\partial\omega}|\mathbf{E_{0,\parallel}}|^2d^{d-1}r\right]^2\sigma_3^{\max}}, \tag{11}$$

where $\eta_0\approx 120\pi\,\Omega$ is the free-space impedance and $\sigma_3^{\max}$ is the maximum value of σ_3 everywhere. The definition of κ_s is directly analogous to Eq. (6) for κ_b with one noteworthy difference: the denominator contains both electric and magnetic fields. We must retain the magnetic field in the denominator of κ_s since the presence of the complex conductivity disturbs the equality of electric and magnetic energies on resonance. Note also that the (c_0/ω_0) scaling factor is in the $d+1$ power, keeping κ_s dimensionless. Using Eq. (11), we can write Eq. (10) as

$$\Delta\omega_s = j\left(\frac{\omega_0}{c_0}\right)^{d+1}\kappa_s\frac{\sigma_3^{\max}}{\varepsilon_0^2}W. \tag{12}$$

$\Delta\omega_s$ has the same form as $\Delta\omega_b$. The presence of the imaginary unit j combined with a purely imaginary σ_3 leads to a negative frequency shift ($\sigma_{3,\mathrm{Im}}>0$) proportional to the stored energy in the cavity, as would be the case for a self-focusing ($n_2>0$) bulk material [cf. Eq. (5)].

It is now important to demonstrate that the last integral in the denominator of Eq. (10) is indeed proportional to the energy stored in the current density (i.e., in graphene), meaning that the entire denominator corresponds to the total stored energy. This can be shown by resorting to the time-domain Poynting theorem and carefully calculating the $\mathcal{J}\cdot\mathcal{E}$ term. In the case of purely real conductivity, this term would account for resistive losses; however, the surface conductivity of graphene is complex with a large imaginary part. Following Ref. [24], we assume a slowly varying envelope approximation: $\mathcal{E}=\mathrm{Re}\{\mathbf{E}_0(t)\exp(+j\omega_0 t)\}=(\mathbf{E}+\mathbf{E}^*)/2$, $\mathcal{J}=\mathrm{Re}\{\mathbf{J}_0(t)\exp(+j\omega_0 t)\}=(\mathbf{J}+\mathbf{J}^*)/2$, and we calculate the product $\langle\mathcal{J}\cdot\mathcal{E}\rangle=(\mathbf{E}^*\cdot\mathbf{J}+\mathbf{E}\cdot\mathbf{J}^*)/4$, with $\langle\cdot\rangle$ denoting time averaging within a period of $T_0=2\pi/\omega_0$. Fourier-transforming the envelope $\mathbf{J_0}(t)$, using Ohm's law, expanding the conductivity in Taylor series, and applying the inverse Fourier transform in the result, we find

$$\langle\mathcal{J}\cdot\mathcal{E}\rangle=\frac{1}{2}\overline{\sigma}^{(1)}_{\mathrm{Re}}\mathbf{E}\cdot\mathbf{E}^*+\frac{1}{4}\frac{\partial}{\partial t}\left\{\frac{\partial\overline{\sigma}^{(1)}_{\mathrm{Im}}}{\partial\omega}\mathbf{E}\cdot\mathbf{E}^*\right\}. \tag{13}$$

A detailed derivation of Eq. (13) can be found in Appendix A. Clearly, the first term on the right-hand side of Eq. (13) expresses power loss density. The second term, on the other hand, describes the rate of change of the energy density stored by the current distribution due to the imaginary part of the electrical conductivity tensor. It thus allows us to define the total surface energy stored in an infinitesimally thin graphene sheet as

$$W_j=\frac{1}{4}\int\frac{\partial\sigma_{1,\mathrm{Im}}}{\partial\omega}|\mathbf{E_{0,\parallel}}|^2d^{d-1}r. \tag{14}$$

Note that when $\sigma_{1,\mathrm{Im}}$ is constant with frequency (dispersionless) this term vanishes, i.e., $W_j=0$ (on the contrary, losses exist regardless of dispersion). However, reactive power consumed in graphene is always nonzero, as can be seen from the Poynting theorem [$\mathbf{S}=(1/2)\mathbf{E_0}\times\mathbf{H_0^*}$] in the frequency domain,

$$\begin{aligned}-\int\nabla\cdot\mathbf{S}\,d^dr &= j\frac{1}{2}\omega_0\int\mu_0|\mathbf{H}_0|^2d^dr\\ &\quad-j\frac{1}{2}\omega_0\int\varepsilon_0\varepsilon_r|\mathbf{E}_0|^2d^dr\\ &\quad+j\frac{1}{2}\int|\sigma_{1,\mathrm{Im}}||\mathbf{E_{0,\parallel}}|^2d^{d-1}r\\ &\quad+\frac{1}{2}\int\sigma_{1,\mathrm{Re}}|\mathbf{E_{0,\parallel}}|^2d^{d-1}r\\ &= j(Q_H-Q_E+Q_J)+P_{\mathrm{loss}}.\end{aligned} \tag{15}$$

On resonance, the total reactive power must be zero, i.e., $Q_E=Q_H+Q_J$ (note that irrespective of the harmonic convention, Q_H and Q_J are always of the same sign, which is, moreover, opposite to that of Q_E). Given that $W_m=Q_H/2\omega_0$ and $W_e=Q_E/2\omega_0$ (when permittivity dispersion is neglected), it follows that $W_e\neq W_m$ when a material with complex conductivity is present and thus the total energy should be evaluated as the sum of its three counterparts.

III. NUMERICAL VALIDATION

The nonlinear frequency shift $\Delta\omega_s$ of Eq. (12) can be readily incorporated in a CMT framework to study the response of a nonlinear resonant structure. Here we focus on a coupled resonator-waveguide system and study its bistable behavior. More specifically, we examine a carbon tube traveling-wave (TW) resonator with a radius R, side-coupled to a graphene sheet waveguide through coupling gap g; see Fig. 1(a). Due to the uniformity along the z axis, the dimensionality of the problem drops to $d=2$. The CMT equation describing

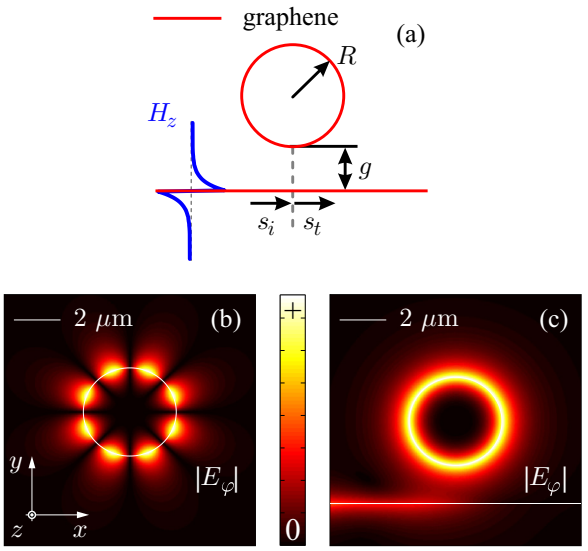

FIG. 1. (a) Infinite carbon tube (TW resonator), side-coupled to an infinite graphene sheet (waveguide). The profile of the TM plasmonic mode supported by the graphene sheet at 10 THz is included. (b) Azimuthal component of the E-field, E_φ, when two degenerate counterpropagating modes are combined with equal weights, resulting in a standing-wave pattern (eigenvalue problem solution). (c) E_φ distribution when a single traveling mode is excited by feeding the bus waveguide.

the resonator-waveguide system at hand is [21,25]

$$\frac{da}{dt} = j(\omega_0 + \Delta\omega_s)a - \left(\frac{1}{\tau_i} + \frac{1}{\tau_e}\right)a + j\sqrt{\frac{2}{\tau_e}}s_i, \qquad (16)$$

where τ_i, τ_e are cavity photon lifetimes corresponding to intrinsic (resistive and radiation) and external (coupling) losses. The respective quality factors are $Q = \omega_0\tau/2$. Cavity amplitude a is normalized so that $|a|^2$ is the stored energy in the cavity, $W = W_e + W_m + W_j$, while incident and transmitted wave amplitudes s_i and s_t (connected through $s_t = s_i + j\sqrt{2/\tau_e}a$) are normalized so that $|s|^2$ expresses guided power.

For the continuous-wave (CW) case, Eq. (16) can be cast in a readily solvable closed-form expression [21], allowing for determining the effect of each system parameter on the nonlinear response gaining physical insight, deriving robust design rules, and specifying the detuning threshold for bistability [13,26]. In short, when the detuning $\delta = (\omega - \omega_0)\tau_i$ is beneath the detuning threshold $\delta_{\text{th}} = -(1 + r_Q)\sqrt{3}$, with $r_Q = Q_i/Q_e$, optical bistability arises: for an appropriate input power, three output states are obtained, with two of them being stable [21]. Input power per unit length for observing bistability is of the order of the characteristic power

$$P_0 = \frac{\varepsilon_0^2 c_0^3}{2\omega_0 \sigma_{3,\text{Im}}^{\max} \kappa_s Q_i^2}, \qquad (17)$$

which must be minimized. Since P_0 is inversely proportional to $\kappa_s Q_i^2$, we seek the parameters maximizing the product.

In Fig. 2 we plot κ_s, Q_i, and P_0 as a function of resonator radius, calculated from linear vectorial finite-element method (VFEM) eigenvalue simulations conducted with COMSOL MULTIPHYSICS®. Note that some attention is required when

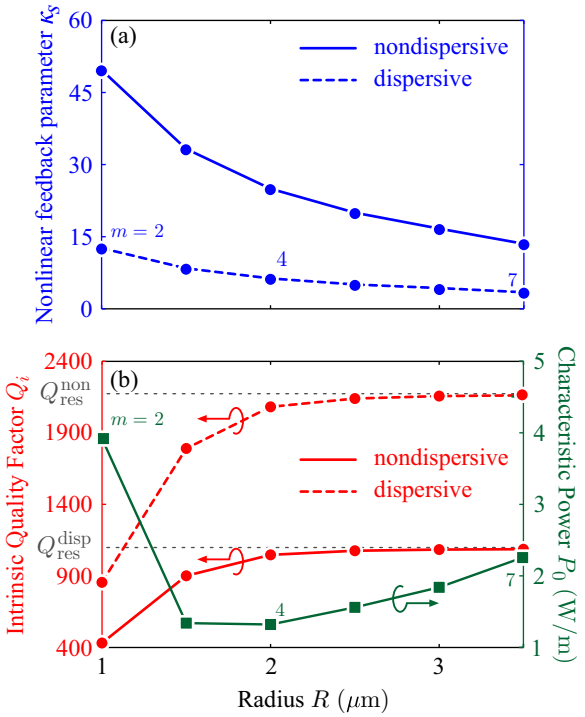

FIG. 2. (a) Nonlinear feedback parameter vs resonator radius R. (b) Intrinsic quality factor and characteristic power vs R. Opposite trends in κ_s and Q_i result in a minimum $P_0 = 1.32$ W/m for $R = 2\ \mu$m. Solid (dashed) lines represent dispersionless (dispersive) cases. P_0 is the same in both cases.

calculating κ_s in TW resonators through an eigenvalue simulation; details can be found in Appendix B. Two cases are considered, one with constant conductivity $\sigma_1 = 0.26 - j560\ \mu$S (solid lines) and one with dispersive conductivity (dashed lines) calculated using Eq. (8) with $\mu_c = 0.3$ eV. In both cases, κ_s decreases with radius because modes with higher azimuthal order m are accompanied by higher effective mode areas, resulting in lower power densities (for a given input power level) and thus weaker electric field amplitudes on graphene. On the other hand, Q_i increases with radius due to the reduced radiation (bending) losses until reaching an upper limit set by resistive losses. To better illustrate this, we distinguish between resistive and radiation losses and compile the corresponding quality factors, Q_{res} and Q_{rad}, in Tables I and II for the dispersive and nondispersive case, respectively.

TABLE I. Uncoupled resonant frequencies along with intrinsic, resistive, and radiation quality factors for the dispersive case. Q_{rad} increases for higher-radial-order modes (larger radius). For $m \geqslant 4$ ($R \geqslant 2\ \mu$m) radiation losses are negligible. Q_{res} is constant with R and limits Q_i.

	$m = 2$	$m = 3$	$m = 4$	$m = 5$	$m = 6$	$m = 7$
R (μm)	1	1.5	2	2.5	3	3.5
f_0 (THz)	10.011	10.018	10.020	10.020	10.021	10.021
Q_i	855	1791	2082	2140	2157	2162
Q_{res}	2167	2167	2167	2166	2166	2166
Q_{rad}	1411	10 302	53 136	$>10^5$	$>10^5$	$>10^5$

TABLE II. Uncoupled resonant frequencies along with intrinsic, resistive, and radiation quality factors for the nondispersive case. Q-factors exhibit an approximately twofold reduction since $W_j = 0$. The behavior with m is the same as in Table I. The different resonance frequency compared with the dispersive case originates from the constant conductivity considered here (calculated at 10 THz).

	$m=2$	$m=3$	$m=4$	$m=5$	$m=6$	$m=7$
R (μm)	1	1.5	2	2.5	3	3.5
f_0 (THz)	9.990	10.003	10.006	10.008	10.009	10.009
Q_i	431	901	1047	1076	1084	1087
Q_{res}	1094	1091	1090	1089	1089	1089
Q_{rad}	711	5183	26 726	87 563	$>10^5$	$>10^5$

Note that the three quality factors (Q_i, Q_{res}, and Q_{rad}) satisfy

$$Q_i = \left(\frac{1}{Q_{\text{res}}} + \frac{1}{Q_{\text{rad}}}\right)^{-1}. \tag{18}$$

Q_{rad} monotonically increases with R as anticipated. For $R \geqslant 2\ \mu$m ($m \geqslant 4$), radiation losses are practically negligible. On the other hand, Q_{res} is constant with R and sets the upper limit in the maximum achievable Q_i.

Given the opposite trends between κ_s and Q_i, minimum characteristic power is obtained for the $m=4$ mode (resonator radius $R = 2\ \mu$m, and unloaded resonance frequency $f_0^{\text{disp}} = 10.020$ THz or $f_0^{\text{non}} = 10.006$ THz for the dispersive and the nondispersive case, respectively), resulting in $P_0 = 1.32$ W/m. For a three-dimensional component with a $\lambda/2$ length along the direction of invariance, the characteristic power is only 20 μW, indicating the potential of graphene for nonlinear applications. To obtain P_0, a value of $\sigma_3 = j4.66 \times 10^{-19}$ S(m/V)^2, calculated through Eq. (9), is used [27]. Importantly, when dispersion is taken into account, κ_s exhibits an approximately fourfold reduction since now $W_j \neq 0$ [Eq. (14)] and the stored energy almost doubles. Accordingly, the quality factor (as evident from its definition $Q_i = \omega_0 W / P_{\text{loss}}$) increases by a factor of ~ 2 (loss remains constant). This is also true for Q_{res} and Q_{rad}. Notably, $P_0^{-1} \propto \kappa_s Q_i^2$ remains unaffected. However, as will be shown in the next paragraph, the impact on the bistability loop when dispersion is neglected is significant.

To complete the design process, we specify that $g = 1.74\ \mu$m is required for critical coupling ($r_Q = 1$). This holds even when dispersion is considered, since both Q_e and Q_i experience an approximately twofold increase and thus r_Q remains constant. Note that critical coupling is essential for achieving high extinction ratios in the bistable loop [21]. The bistability curves, as calculated with the proposed framework for both dispersive and nondispersive graphene, are depicted in Fig. 3 for an operating frequency $f^{\text{disp}} = 10.006$ THz and $f^{\text{non}} = 10$ THz, lower than the unperturbed loaded resonance frequency $f_{0,\text{L}}^{\text{disp}} = 10.027$ THz and $f_{0,\text{L}}^{\text{non}} = 10.021$ THz by $\Delta f = 21$ GHz for both cases. Because of the different Q_i values in the two cases, the normalized detuning is different: $\delta = 1.3\delta_{\text{th}}$ (dispersionless) and $\delta = 2.6\delta_{\text{th}}$ (dispersive), with respect to their common δ_{th} value. This, in turn, significantly impacts the span and position of the bistability loop. As a result, taking graphene dispersion into account is crucial for correctly capturing the nonlinear response and associating with experimental results. To confirm the validity of our framework, we compare the results with full-wave nonlinear VFEM simulations shown with markers in Fig. 3. The two bistable branches are revealed by conducting two different power sweeps, one with ascending and one with descending steps. The solution of each step is used as an initial condition for the next one. Clearly, the agreement between the two methods is exceptional.

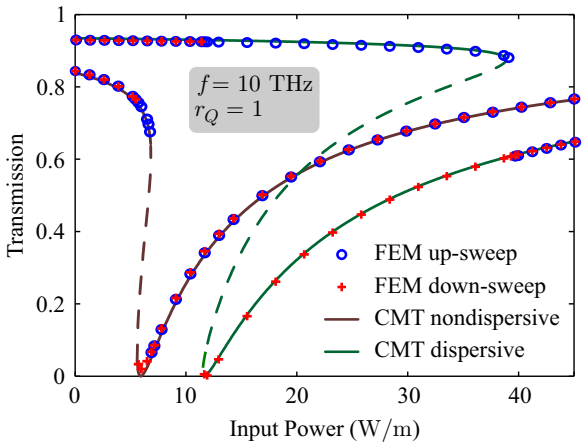

FIG. 3. Bistability curves for dispersive (green) and nondispersive (brown) graphene calculated with the proposed framework at $f^{\text{disp}} = 10.006$ THz ($f_{0,\text{L}}^{\text{disp}} = 10.027$ THz) and $f^{\text{non}} = 10$ THz ($f_{0,\text{L}}^{\text{non}} = 10.021$ THz), respectively. Note the significant impact on the bistability loop. Circular (cross) markers are calculated with the nonlinear VFEM for ascending (descending) input power. The agreement is excellent.

IV. CONCLUSIONS

To recapitulate, we have developed a general framework for nonlinear resonant structures comprising dispersive bulk and sheet materials. Although we have focused on third-order electronic (Kerr) nonlinearity, the proposed framework can handle any arbitrary nonlinearity expressed through the nonlinear current density (or nonlinear polarization) term. Therefore, it paves the way for modeling a multitude of nonlinear phenomena with sheet materials, which have recently found their way into THz/photonic components, and assessing their true potential for nonlinear applications.

Importantly, we have demonstrated that when media with a complex conductivity are involved, such as graphene, the equality of electric and magnetic energies ceases to hold (a condition that is typically taken for granted) and the stored energy must be evaluated as the sum of electric, magnetic, and current density energies. This stems from the reactive power associated with the imaginary part of graphene's surface conductivity. In addition, we have shown that incorporating the dispersion of linear material properties is important since it can significantly impact the nonlinear response. This has been explained in terms of the energy stored in the surface current, which is zeroed out when linear dispersion is neglected.

The proposed framework not only provides physical insight and clear design rules, but it is also accurate and efficient.

It thus allows for modeling large physical systems that would otherwise be too costly to model with full-wave nonlinear simulations. In turn, this facilitates cross-checking with experimental results and performing elaborate design processes for meeting specific component requirements.

ACKNOWLEDGMENTS

This work was supported by the "Research Projects for Excellence, IKY/SIEMENS."

APPENDIX A: STORED ENERGY IN DISPERSIVE GRAPHENE

In this appendix, we will derive Eq. (13) by following Ref. [24]. The Poynting theorem in the time domain is

$$-\nabla\cdot(\boldsymbol{\mathcal{E}}\times\boldsymbol{\mathcal{H}})=\boldsymbol{\mathcal{J}}\cdot\boldsymbol{\mathcal{E}}+\boldsymbol{\mathcal{E}}\cdot\frac{\partial\boldsymbol{\mathcal{D}}}{\partial t}+\boldsymbol{\mathcal{H}}\cdot\frac{\partial\boldsymbol{\mathcal{B}}}{\partial t}. \tag{A1}$$

The second and third terms on the right-hand side of Eq. (A1) correspond to the rate of change of the stored energy density. The total stored electric and magnetic energies in dispersive media are given by the widely known expressions [24]

$$\begin{aligned}W_e&=\int\left(\int\boldsymbol{\mathcal{E}}\cdot\frac{\partial\boldsymbol{\mathcal{D}}}{\partial t}dt\right)d^dr\\&=\frac{1}{4}\int\left.\frac{\partial\{\omega\bar{\varepsilon}(\omega)\}}{\partial\omega}\right|_{\omega=\omega_0}\mathbf{E}\cdot\mathbf{E}^*d^dr,\end{aligned} \tag{A2a}$$

$$\begin{aligned}W_m&=\int\left(\int\boldsymbol{\mathcal{H}}\cdot\frac{\partial\boldsymbol{\mathcal{B}}}{\partial t}dt\right)d^dr\\&=\frac{1}{4}\int\left.\frac{\partial\{\omega\overline{\mu}(\omega)\}}{\partial\omega}\right|_{\omega=\omega_0}\mathbf{H}\cdot\mathbf{H}^*d^dr.\end{aligned} \tag{A2b}$$

The first term on the right-hand side of Eq. (A1), on the other hand, usually corresponds to power loss density. This is true only when the conductivity tensor is purely real. In the case of materials with complex conductivity (such as graphene), it results in an extra term describing the rate of change of the energy stored in the imaginary part of the dispersive conductivity tensor. To show this, let us assume a slowly varying envelope approximation for both the electric field and current density, i.e.,

$$\boldsymbol{\mathcal{E}}=\mathrm{Re}\{\mathbf{E}_0(t)e^{+j\omega_0t}\}=\mathrm{Re}\{\mathbf{E}\}=\frac{(\mathbf{E}+\mathbf{E}^*)}{2}, \tag{A3a}$$

$$\boldsymbol{\mathcal{J}}=\mathrm{Re}\{\mathbf{J}_0(t)e^{+j\omega_0t}\}=\mathrm{Re}\{\mathbf{J}\}=\frac{(\mathbf{J}+\mathbf{J}^*)}{2}. \tag{A3b}$$

Substituting Eqs. (A3) in the first term of Eq. (A1) and applying time averaging (denoted by $\langle\cdot\rangle$) within a period of $T_0=2\pi/\omega_0$, we get

$$\langle\boldsymbol{\mathcal{J}}\cdot\boldsymbol{\mathcal{E}}\rangle=\frac{(\mathbf{E}^*\cdot\mathbf{J}+\mathbf{E}\cdot\mathbf{J}^*)}{4}. \tag{A4}$$

The slowly varying envelope can be expressed in the frequency domain using Fourier transformation, resulting in the following expression for the current:

$$\mathbf{J}=\mathbf{J}_0(t)e^{j\omega_0t}=\left[\frac{1}{2\pi}\int_{-\infty}^{\infty}\tilde{\mathbf{J}}_0(\xi)e^{j\xi t}d\xi\right]e^{j\omega_0t}, \tag{A5}$$

with ξ being the baseband frequency. $\tilde{\mathbf{J}}_0(\xi)$ and $\tilde{\mathbf{E}}_0(\xi)$ are related by Ohm's law through $\tilde{\mathbf{J}}_0(\xi)=[\overline{\sigma}^{(1)}_{\mathrm{Re}}(\xi+\omega_0)+j\overline{\sigma}^{(1)}_{\mathrm{Im}}(\xi+\omega_0)]\tilde{\mathbf{E}}_0(\xi)$. Note that the value of $\overline{\sigma}^{(1)}$ at the "high" frequency $\omega=\xi+\omega_0$ is used. To proceed, we use a zeroth-order Taylor series expansion for the real part of electrical conductivity (i.e., we neglect dispersion of losses) and a first-order Taylor series expansion for the imaginary part, both around $\xi=0$,

$$\overline{\sigma}^{(1)}_{\mathrm{Re}}(\xi+\omega_0)\approx\overline{\sigma}^{(1)}_{\mathrm{Re}}(\omega_0), \tag{A6a}$$

$$\begin{aligned}\overline{\sigma}^{(1)}_{\mathrm{Im}}(\xi+\omega_0)&\approx\overline{\sigma}^{(1)}_{\mathrm{Im}}(\omega_0)+\xi\left.\frac{\partial\{\overline{\sigma}^{(1)}_{\mathrm{Im}}(\xi+\omega_0)\}}{\partial\xi}\right|_{\xi=0}\\&=\overline{\sigma}^{(1)}_{\mathrm{Im}}(\omega_0)+\xi\left.\frac{\partial\overline{\sigma}^{(1)}_{\mathrm{Im}}(\omega)}{\partial\omega}\right|_{\omega=\omega_0}.\end{aligned} \tag{A6b}$$

Substituting Eqs. (A6) in Eq. (A5), we reach

$$\begin{aligned}\mathbf{J}=&\left[\frac{1}{2\pi}\overline{\sigma}^{(1)}_{\mathrm{Re}}(\omega_0)\int_{-\infty}^{\infty}\tilde{\mathbf{E}}_0(\xi)e^{j\xi t}d\xi\right]e^{j\omega_0t}\\&+\left[j\frac{1}{2\pi}\overline{\sigma}^{(1)}_{\mathrm{Im}}(\omega_0)\int_{-\infty}^{\infty}\tilde{\mathbf{E}}_0(\xi)e^{j\xi t}d\xi\right]e^{j\omega_0t}\\&+\left[\frac{1}{2\pi}\frac{\partial\overline{\sigma}^{(1)}_{\mathrm{Im}}(\omega)}{\partial\omega}\int_{-\infty}^{\infty}j\xi\tilde{\mathbf{E}}_0(\xi)e^{j\xi t}d\xi\right]e^{j\omega_0t}.\end{aligned} \tag{A7}$$

Note that all the derivatives involved are calculated at $\omega=\omega_0$. In the last integral on the right-hand side of Eq. (A7), we recognize that the term $j\xi\tilde{\mathbf{E}}_0(\xi)\exp(j\xi t)$ can alternatively be written as $\partial\{\tilde{\mathbf{E}}_0(\xi)\exp(j\xi t)\}/\partial t$. By mutually exchanging integral and differential operators and applying inverse Fourier transformation, we get

$$\begin{aligned}\mathbf{J}=&\,\overline{\sigma}^{(1)}_{\mathrm{Re}}(\omega_0)\mathbf{E}_0(t)e^{j\omega_0t}+j\overline{\sigma}^{(1)}_{\mathrm{Im}}(\omega_0)\mathbf{E}_0(t)e^{j\omega_0t}\\&+\frac{\partial\overline{\sigma}^{(1)}_{\mathrm{Im}}(\omega)}{\partial\omega}\frac{\partial\{\mathbf{E}_0(t)\}}{\partial t}e^{j\omega_0t}.\end{aligned} \tag{A8}$$

Finally, returning to Eq. (A4) and substituting Eq. (A8), we arrive at Eq. (13):

$$\langle\boldsymbol{\mathcal{J}}\cdot\boldsymbol{\mathcal{E}}\rangle=\frac{1}{2}\overline{\sigma}^{(1)}_{\mathrm{Re}}(\omega_0)\mathbf{E}\cdot\mathbf{E}^*+\frac{1}{4}\frac{\partial}{\partial t}\left\{\frac{\partial\overline{\sigma}^{(1)}_{\mathrm{Im}}(\omega)}{\partial\omega}\mathbf{E}\cdot\mathbf{E}^*\right\}. \tag{A9}$$

As already mentioned, the first term on the right-hand side of Eq. (A9) expresses power loss density. On the other hand, the second term describes the rate of change of the energy density stored by the current distribution due to the imaginary part of the electrical conductivity tensor. In accordance with Eqs. (A2), we can define the total stored energy as

$$W_j=\frac{1}{4}\int\left.\frac{\partial\overline{\sigma}^{(1)}_{\mathrm{Im}}(\omega)}{\partial\omega}\right|_{\omega=\omega_0}\mathbf{E}\cdot\mathbf{E}^*d^dr. \tag{A10}$$

Equation (14) is a simplified version of Eq. (A10) when graphene is the only material with imaginary conductivity involved.

APPENDIX B: CORRECT ESTIMATION OF THE NONLINEAR FEEDBACK PARAMETER IN TRAVELING-WAVE RESONATORS

Estimating the value of κ through Eq. (6) or Eq. (11) in a TW resonator requires some attention if the solution of an eigenvalue problem is used for obtaining the mode distribution (the alternative is to use a weakly coupled harmonic propagation simulation and exclude the waveguide from the integration domain). Specifically, the solution of the eigenvalue simulation is typically a standing wave (SW) consisting of the two degenerate counterpropagating modes with equal weights [Fig. 1(b)], instead of a unidirectional TW mode [Fig. 1(c)]. This affects the calculated κ, as can be easily shown.

Let us begin by assuming that a single traveling wave in the resonator, propagating in a counterclockwise direction, can be expressed as

$$\mathbf{e}^{+}(\rho,\varphi) = [e_\rho(\rho)\hat{\boldsymbol{\rho}} + je_\varphi(\rho)\hat{\boldsymbol{\varphi}}]e^{-jm\varphi}, \tag{B1}$$

where $e_{\rho,\varphi}(\rho)$ are the E-field components and m is the azimuthal order of the resonant mode. The $\pi/2$ phase difference between transverse and axial components holds exactly for lossless waveguides [18]. However, we have verified that this holds in our case as well; this is because the field components do not overlap with a lossy material. For a wave propagating in a clockwise direction, we have

$$\mathbf{e}^{-}(\rho,\varphi) = [e_\rho(\rho)\hat{\boldsymbol{\rho}} - je_\varphi(\rho)\hat{\boldsymbol{\varphi}}]e^{+jm\varphi}. \tag{B2}$$

Similar expressions can be written for the magnetic field, i.e., $\mathbf{h}^{\pm} = \mp h_z(\rho)\hat{\mathbf{z}}e^{\mp jm\varphi}$.

In the solution of the eigenvalue problem, the total electric field on resonance consists of a linear combination of Eqs. (B1) and (B2) with equal weights, i.e.,

$$\mathbf{E}_{\mathbf{0}}^{\mathbf{eig}} = \mathbf{e}^{+} + \mathbf{e}^{-} = 2e_\rho\cos(m\varphi)\hat{\boldsymbol{\rho}} + 2e_\varphi\sin(m\varphi)\hat{\boldsymbol{\varphi}}. \tag{B3}$$

The tangential to the graphene sheet electric field is

$$\mathbf{E}_{\mathbf{0},\parallel}^{\mathbf{eig}} = 2e_\varphi\sin(m\varphi)\hat{\boldsymbol{\varphi}}. \tag{B4}$$

On the other hand, for the single unidirectional mode in a harmonic propagation simulation, it simply holds that $\mathbf{E}_{\mathbf{0}}^{\mathbf{prop}} = \mathbf{e}^{+}$. Similarly, for the magnetic field we have $\mathbf{H}_{\mathbf{0}}^{\mathbf{eig}} = \mathbf{h}^{+} + \mathbf{h}^{-} = -2jh_z\sin(m\varphi)\hat{\mathbf{z}}$ and $\mathbf{H}_{\mathbf{0}}^{\mathbf{prop}} = \mathbf{h}^{+}$, respectively.

To calculate the nonlinear feedback parameter κ_s through Eq. (11), we have to calculate various norms of the electric and magnetic field presented below,

$$\left|\mathbf{E}_{\mathbf{0}}^{\mathbf{eig}}\right|^2 = 4|e_\rho|^2\cos^2(m\varphi) + 4|e_\varphi|^2\sin^2(m\varphi), \tag{B5a}$$

$$\left|\mathbf{H}_{\mathbf{0}}^{\mathbf{eig}}\right|^2 = 4|h_z|^2\sin^2(m\varphi), \tag{B5b}$$

$$\left|\mathbf{E}_{\mathbf{0},\parallel}^{\mathbf{eig}}\right|^2 = 4|e_\varphi|^2\sin^2(m\varphi), \tag{B5c}$$

$$\left|\mathbf{E}_{\mathbf{0},\parallel}^{\mathbf{eig}}\right|^4 = 16|e_\varphi|^4\sin^4(m\varphi), \tag{B5d}$$

$$\left|\mathbf{E}_{\mathbf{0},\parallel}^{\mathbf{eig}}\cdot\mathbf{E}_{\mathbf{0},\parallel}^{\mathbf{eig}}\right|^2 = 16\left|e_\varphi^2\right|^2\sin^4(m\varphi), \tag{B5e}$$

$$\left|\mathbf{E}_{\mathbf{0}}^{\mathbf{prop}}\right|^2 = |e_\rho|^2 + |e_\varphi|^2, \tag{B5f}$$

$$\left|\mathbf{H}_{\mathbf{0}}^{\mathbf{prop}}\right|^2 = |h_z|^2, \tag{B5g}$$

$$\left|\mathbf{E}_{\mathbf{0},\parallel}^{\mathbf{prop}}\right|^2 = |e_\varphi|^2, \tag{B5h}$$

$$\left|\mathbf{E}_{\mathbf{0},\parallel}^{\mathbf{prop}}\right|^4 = |e_\varphi|^4, \tag{B5i}$$

$$\left|\mathbf{E}_{\mathbf{0},\parallel}^{\mathbf{prop}}\cdot\mathbf{E}_{\mathbf{0},\parallel}^{\mathbf{prop}}\right|^2 = \left|e_\varphi^2\right|^2. \tag{B5j}$$

Substituting Eqs. (B5) in Eq. (11), performing the integration with respect to φ, and taking into account that $\int_0^{2\pi}\cos^2(m\varphi)d\varphi = \int_0^{2\pi}\sin^2(m\varphi)d\varphi = \pi$, $\int_0^{2\pi}\sin^4(m\varphi)d\varphi = 3\pi/4$ for any integer $m \neq 0$ and $\int_0^{2\pi} d\varphi = 2\pi$, we get (for the $d = 2$ case)

$$\kappa_s^{\mathrm{eig}} = \frac{3\pi/4}{\pi^2}\left(\frac{c_0}{\omega_0}\right)^3 \frac{3\sigma_3|e_\varphi(R)|^4 R}{\left[\int \varepsilon_r(|e_\rho|^2 + |e_\varphi|^2)\rho\, d\rho + \int \eta_0^2|h_z|^2\rho\, d\rho + \frac{1}{\varepsilon_0}\frac{\partial\sigma_{1,\mathrm{Im}}}{\partial\omega}|e_\varphi(R)|^2 R\right]^2\sigma_3^{\max}}, \tag{B6a}$$

$$\kappa_s^{\mathrm{prop}} = \frac{2\pi}{(2\pi)^2}\left(\frac{c_0}{\omega_0}\right)^3 \frac{3\sigma_3|e_\varphi(R)|^4 R}{\left[\int \varepsilon_r(|e_\rho|^2 + |e_\varphi|^2)\rho\, d\rho + \int \eta_0^2|h_z|^2\rho\, d\rho + \frac{1}{\varepsilon_0}\frac{\partial\sigma_{1,\mathrm{Im}}}{\partial\omega}|e_\varphi(R)|^2 R\right]^2\sigma_3^{\max}}. \tag{B6b}$$

Taking the ratio of the two quantities, we find

$$\frac{\kappa_s^{\mathrm{eig}}}{\kappa_s^{\mathrm{prop}}} = \frac{3}{2}. \tag{B7}$$

The result of Eq. (B7) indicates that when using an eigenvalue simulation to calculate κ_s in a TW resonator, we have to correct the result by a factor of $2/3$, originating from the different field distributions of the traveling- and standing-wave patterns.

[1] T. Tanabe, M. Notomi, S. Mitsugi, A. Shinya, and E. Kuramochi, Opt. Lett. **30**, 2575 (2005).

[2] S. F. Mingaleev, A. E. Miroshnichenko, Y. S. Kivshar, and K. Busch, Phys. Rev. E **74**, 046603 (2006).

[3] M. F. Yanik, S. Fan, M. Soljačić, and J. D. Joannopoulos, Opt. Lett. **28**, 2506 (2003).

[4] J. Wang, L. Fan, L. T. Varghese, H. Shen, Y. Xuan, B. Niu, and M. Qi, J. Lightw. Technol. **31**, 313 (2013).

[5] Q. Xu and M. Lipson, Opt. Express **15**, 924 (2007).

[6] S. Malaguti, G. Bellanca, A. de Rossi, S. Combrié, and S. Trillo, Phys. Rev. A **83**, 051802 (2011).
[7] T. Van Vaerenbergh, M. Fiers, J. Dambre, and P. Bienstman, Phys. Rev. A **86**, 063808 (2012).
[8] T. Gu, N. Petrone, J. F. McMillan, A. van der Zande, M. Yu, G. Q. Lo, D. L. Kwong, J. Hone, and C. W. Wong, Nat. Photon. **6**, 554 (2012).
[9] A. Y. Nikitin, T. Low, and L. Martin-Moreno, Phys. Rev. B **90**, 041407 (2014).
[10] C. Horvath, D. Bachman, R. Indoe, and V. Van, Opt. Lett. **38**, 5036 (2013).
[11] M. Soljačić, M. Ibanescu, S. G. Johnson, Y. Fink, and J. D. Joannopoulos, Phys. Rev. E **66**, 055601 (2002).
[12] J. Bravo-Abad, S. Fan, S. Johnson, J. D. Joannopoulos, and M. Soljačić, J. Lightw. Technol. **25**, 2539 (2007).
[13] O. Tsilipakos, T. Christopoulos, and E. E. Kriezis, J. Lightw. Technol. **34**, 1333 (2016).
[14] D. Chatzidimitriou, A. Pitilakis, and E. E. Kriezis, J. Appl. Phys. **118**, 023105 (2015).
[15] S. A. Mikhailov and K. Ziegler, J. Phys.: Condens. Matter **20**, 384204 (2008).
[16] P. N. Butcher and D. Cotter, *The Elements of Nonlinear Optics* (Cambridge University Press, Cambridge, 1990).
[17] S. V. Afshar and T. M. Monro, Opt. Express **17**, 2298 (2009).
[18] A. W. Snyder and J. D. Love, *Optical Waveguide Theory* (Chapman and Hall, New York, 1983).
[19] C. Sauvan, J. P. Hugonin, I. S. Maksymov, and P. Lalanne, Phys. Rev. Lett. **110**, 237401 (2013).
[20] This is naturally satisfied for any computational domain when radiation losses are negligible (note that we consider an uncoupled resonator since for the purpose of specifying the nonlinear frequency shift, the presence of the waveguide is only a slight perturbation to the field distribution). This is exactly the case with the carbon tube resonator that will be investigated in the numerical example of Sec. III for azimuthal order $m \geqslant 3$, as evident from the corresponding radiation quality factors compiled in Tables I and II. When radiation losses become significant, the boundary integral ceases to be zero unless a specific computational domain is adopted, i.e., perfectly matched layers are employed backed with a hard-wall boundary condition. In addition, there is significant energy stored in the radiation leakage that moreover depends on the size of the computational domain. To properly handle such cases, the proposed framework should be adjusted accordingly. Modifications can be sought in extending the d-dimensional integration inside the perfectly matched layers and making use of the unconjugated reciprocity theorem, as done in Ref. [19] in the context of calculating spontaneous emission rates.
[21] O. Tsilipakos and E. E. Kriezis, J. Opt. Soc. Am. B **31**, 1698 (2014).
[22] G. W. Hanson, IEEE Trans. Antennas Propag. **56**, 747 (2008).
[23] L. A. Falkovsky, Phys. Usp. **51**, 887 (2008).
[24] L. D. Landau, L. P. Pitaevskii, and E. M. Lifshitz, *Electrodynamics of Continuous Media*, 2nd ed. (Elsevier Butterworth-Heinemann, Oxford, 1984).
[25] H. A. Haus, *Waves and Fields in Optoelectronics* (Prentice-Hall, Englewood Cliffs, NJ, 1984).
[26] T. Christopoulos, G. Sinatkas, O. Tsilipakos, and E. E. Kriezis, Opt. Quantum Electron. **48**, 128 (2016).
[27] Having modeled graphene as an infinitesimally thin material, σ_3 is the natural parameter for describing material nonlinearity. For the sole purpose of comparing with bulk materials, we can define an equivalent n_2 parameter. Assuming a typical thickness of 0.34 nm and using the expression found in Ref. [14], we find $n_2^{\text{equiv}} = 2 \times 10^{-13}\ \text{m}^2/\text{W}$. This value is four orders of magnitude higher than those of bulk nonlinear materials (semiconductors, nonlinear polymers, and chalcogenide glasses), which can be considered indicative of the potential of graphene as a nonlinear material.